crystals

MDPI

Article

Preparation of Niobium Aluminium Alloy Based on Shock Compression Method

Ya-Le Tao [1], Zhen Jiao [1], Zheng-Tang Liu [2], Cheng-Lu Jiang [3,*] and Qi-Jun Liu [1,*]

[1] Bond and Band Engineering Group, Southwest Jiaotong University, Chengdu 610031, China; abc446@sina.com (Y.-L.T.); z.jiao@utwente.nl (Z.J.)
[2] State Key Laboratory of Solidification Processing, Northwestern Polytechnical University, Xi'an 710072, China; liuzht@nwpu.edu.cn
[3] College of Water Conservancy and Hydropower Engineering, Sichuan Agricultural University, Ya'an 625014, China
* Correspondence: juul@my.swjtu.edu.cn (C.-L.J.); qijunliu@home.swjtu.edu.cn (Q.-J.L.)

Abstract: A new method based on a light-gas gun has been proposed to synthesize Nb-Al alloys, and a recovery capsule has been investigated. The copper-coated sample is accessible after shock wave loading. In this paper, we successfully synthesize Nb-Al alloys, which are high-temperature structural materials. X-ray diffraction is employed to clarify the structural characteristics of compounds after impact, and the simulation of X-ray diffractions is employed to clarify the structure. In detail, tetragonal $NbAl_3$ alloys certainly appeared in the recovery capsule; this alloy is considered to be best candidate.

Keywords: shock wave loading; $NbAl_3$ alloys; X-ray diffractions

check for updates

Citation: Tao, Y.-L.; Jiao, Z.; Liu, Z.-T.; Jiang, C.-L.; Liu, Q.-J. Preparation of Niobium Aluminium Alloy Based on Shock Compression Method. *Crystals* **2022**, *12*, 381. https://doi.org/10.3390/cryst12030381

Academic Editor: Sergio Brutti

Received: 25 February 2022
Accepted: 10 March 2022
Published: 12 March 2022

Publisher's Note: MDPI stays neutral with regard to jurisdictional claims in published maps and institutional affiliations.

Copyright: © 2022 by the authors. Licensee MDPI, Basel, Switzerland. This article is an open access article distributed under the terms and conditions of the Creative Commons Attribution (CC BY) license (https://creativecommons.org/licenses/by/4.0/).

1. Introduction

As one of the dynamic high-pressure loading devices, a light-gas gun can realize high-temperature and high-pressure conditions by the collision of a projectile with a target [1]. In 1946, the United States successfully developed the first light gas gun; it has become an important tool for studying the equation of state of materials under high pressure, the electromagnetic properties, the impact of new materials, the simulation of high-speed collision planetary, etc. [2–4]. Compared with conventional synthesis methods, shock wave synthesis technology caused by light-gas guns has the advantages of fast loading time, uniform pressure distribution, fine particle size and good sintering performance [3,4].

To the best of our knowledge, there are a lot of newly formed materials and new compression-induced phases under shock compression. For instance, diamond, wurtzite-type BN and spinel-type nitrides and a new phase of carbon nitrides were synthesized via shock wave [5–8]. Moreover, the Hugoniot relations of spinel-type ceramics of Fe_3O_4 and AlON suggested that the post-spinel phases could be formed above 100 GPa [9,10].

Nb-Al alloys recently attracted wide attention as high-temperature structural materials due to their low density, high melting point, high toughness and excellent high temperature strength [11,12]. It is well known that the Nb-Al binary system consists of Nb_3Al, Nb_2Al and $NbAl_3$ intermetallics [13,14]. Among them, there is no literature to show the preparation of Nb-Al alloys under shock waves produced by light-gas guns. Nevertheless, the structural analogue A15 Nb_3Si was synthesized using a two-stage light-gas gun [15]. In the reaction-assisted shock consolidation of Nb-Al alloys, the $NbAl_3$ and Nb_2Al compounds were identified with X-ray diffraction. Unfortunately, as the plane wave caused by the chemical-induced shock was not uniform, the products were mixed with other impurities [16]. To obtain high-quality alloys, model experiments were planned and carried out using a two-stage light-gas gun.

2. Experimental Methods

The experimental device is schematically shown in Figure 1 [17]. The diameter and thickness of the reaction chamber's geometrical dimensions (first warehouse) were 12.1 mm and 4 mm, respectively. The copper flyer with 3 mm thickness and recovery capsule in synthesis section collided with each other with a flyer velocity that ranged from 1200 to 3300 m/s, caused by a two-stage light-gas gun. As far as we know, copper is generally chosen to synthesize and recover high-pressure phases because copper is known for having high shock-impedance and thermal conductivity. The original samples were prepared by mixing 99.95% pure niobium powder and 99.95% pure aluminum powder, and the mass ratio 60:40 of Nb:Al mixture ratio was mixed under nitrogen atmosphere. Additionally, then the original samples were made into a 12 mm diameter sheet sample (cylindrical, of 3.81×10^3 kg/m^3 density) via preforming. The purpose of this step was to prevent the aluminium powder from deflagration and to avoid the oxidation of the samples. To ensure that the shock wave generated by high-speed collision passed through the sample to achieve the maximum balance pressure, a high-quality steel frame was used to fix the recovery capsule. As shown in Figure 2 [18], all samples were placed in the first warehouse of the recovery capsule, which included a pedestal and a screw cap. In order to avoid the effects of sparse waves, the pedestal and screw cap were made of the same material. Six samples came from same batch; the considered parameters are listed in Table 1. Finally, the recovered samples were characterized using X-ray diffraction. The X'Pert Pro MPD X was used; the manufacturer of the X-ray was HollandPanalytical (Almelo, The Netherlands).

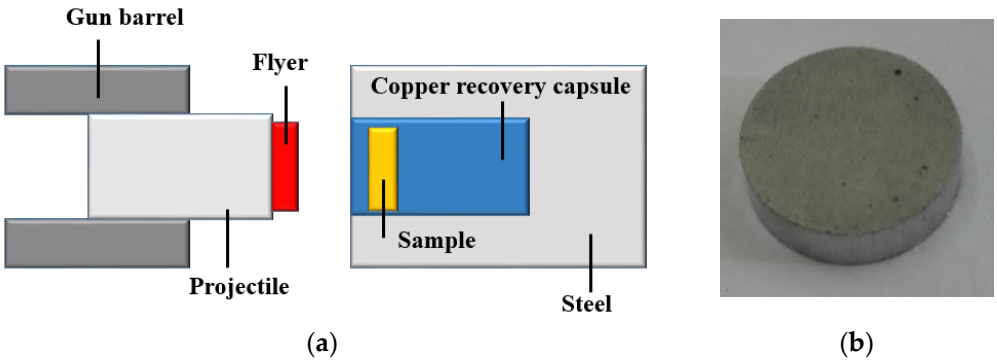


Figure 1. Schematic of the reaction chamber connected to the part of light-gas gun (**a**), sample (**b**) [17].

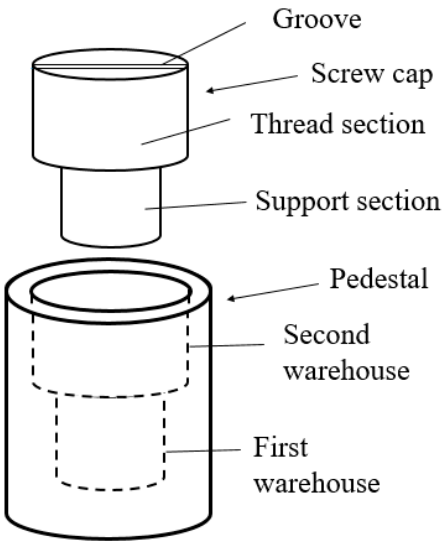


Figure 2. The schematic of recovery capsule [18].

Table 1. Parameters of Nb and Al powder compact.

Number	Diameter (mm)	Thickness (mm)	Mass (g)	Density	Porosity
No. 1	12	3.16	1.361	3.81	38.8%
No. 2	12	3.21	1.382	3.81	38.8%
No. 3	12	3.56	1.537	3.82	38.6%
No. 4	12	3.36	1.455	3.82	38.6%
No. 5	12	3.54	1.526	3.81	38.8%
No. 6	12	3.26	1.408	3.81	38.8%

The X-ray diffraction calculations of Nb-Al alloys were performed using the first principles implemented in the CASTEP (Cambridge Serial Total Energy Package) code [19,20]. The diffraction peaks were applied based on the Pseudo-Voight function. The models for diffraction simulation in this paper were tetragonal $NbAl_3$, whose parameters are a = 3.8458 Å, c = 8.6094 Å [21], and cubic Nb_7Al, whose parameters are a = 3.275 Å [22]. The lattice parameter of pure cubic metal model for Nb is a = 3.3 Å [23], for Al it is a = 4.056 Å [24], and for Cu it is a = 3.613 Å [25], respectively.

3. Results and Discussion

As shown in Table 2, the alloys were synthesized with different impact velocities. The impact pressures were calculated using the Hugoniot equation $P = \rho(C_0 + \lambda\mu)\mu$ [26], where the Hugoniot parameter of copper is C_0 = 3.933 km/s and λ = 1.5 [27]. The density ρ of copper is 8.93 g/cm^3. The impact velocity μ is expressed by the symmetric collision equation $\mu = \frac{W}{2}$ [28], where the W is the velocity of flyer measured with the magnetic speed measuring system. One copper recovery capsule and copper-coated samples are shown as examples in Figure 3; it can be seen that the recovery capsule is geometrically maintained. The powder compact after shock wave loading was very thin and had a metal lustre.

Table 2. The shock compression loading parameters at different impact velocities.

Number.	Mass of Sheet (g)	Impact Velocity (km/s)	Impact Pressure (GPa)
No. 1	1.361	2.14	44.31
No. 2	1.382	1.63	31.79
No. 3	1.537	2.52	54.44
No. 4	1.45	1.28	23.91
No. 5	1.526	2.60	56.65
No. 6	1.408	3.28	86.91

Figures 4 and 5 show the X-ray data of sample No. 3 and sample No. 5, respectively. Each substance is represented by a colour. Comparison of the shape and size of these diffraction peaks implies that the $NbAl_3$ and Nb_7Al were successfully synthesized. Interestingly, the $NbAl_3$ compound was produced in both two different impact velocities. A strong peak appeared in the 2θ range of 38 to 40°, which corresponded to the (112) surface. It is suggested that the $NbAl_3$ (112) is the most easily synthetic plane in Nb-Al alloys. The characteristics of $NbAl_3$ alloy synthesized at 2.52 km/s are comparable to that of the alloy synthesized at 2.6 km/s, where the (204) surface and (004) surface appear at different impact velocities, respectively. The impact of a shock wave travelling with sufficient velocity would impart enough energy to promote the shock synthesis of alloys.



(**a**) (**b**)

Figure 3. Copper recovery capsule (**a**), copper-coated sample (**b**) after undergoing shock wave loading.

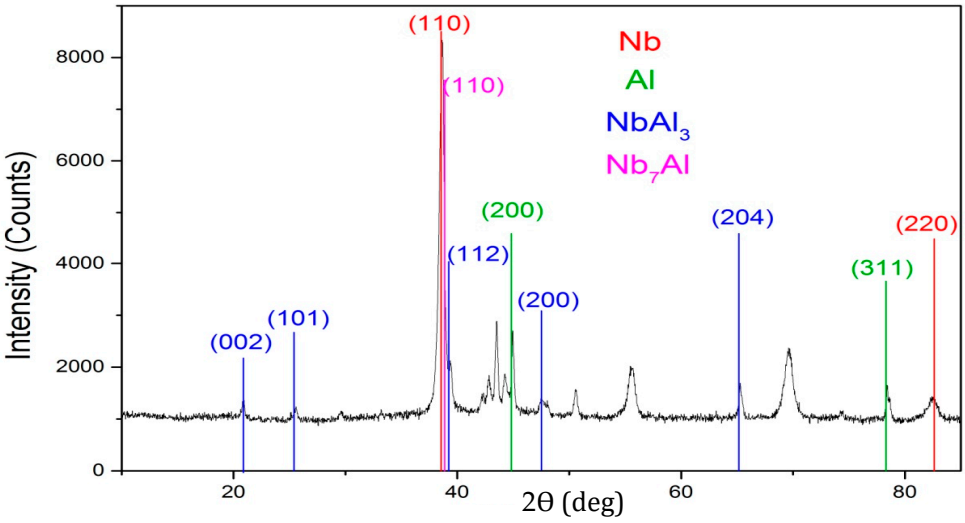


Figure 4. The X-ray diffraction for 2.52 km/s specimen.

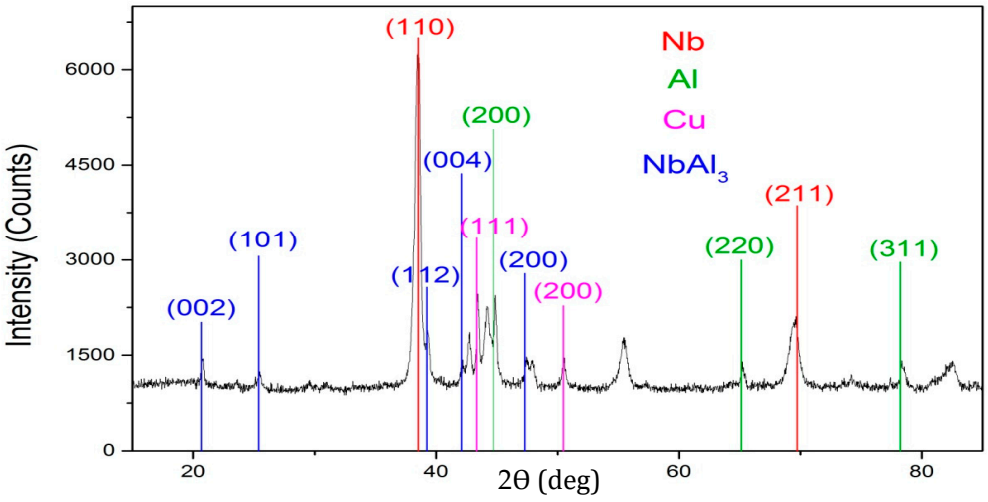


Figure 5. The X-ray diffraction for 2.60 km/s specimen.

To support our experimental observation of alloys, the structure and reflex powder diffraction were studied based on the Pseudo-Voight function. The crystal models of I4/mmm $NbAl_3$, Im-3m Nb_7Al, Im-3m Nb, Fm-3m Al and Fm-3m Cu were built for X-ray

diffraction simulation. Simulated diffraction images compared with X-ray data are shown in Figures 4 and 5. In all, the X-ray diffraction peaks of Nb-Al alloys included $NbAl_3$ and Nb_7Al. In detail, the pure metal Nb (110) had a diffraction peak in the 2θ at 38°, and the pure metal Al (200), (311) and (220) had diffraction peaks in the 2θ at 44, 65 and 78°, respectively. The experimental peaks of pure metals indicate that the synthesis of Nb-Al alloys contained the residual metal power. Copper (111) and (200) peaks in the 2θ at 42 and 45° revealed that copper permeated to Nb-Al alloys under impact. At an impact velocity of 2.52 km/s, it can be seen that the plane (112) of $NbAl_3$ and the plane (110) of Nb_7Al overlapped with pure cubic Nb, because they have the same atomic distributions in plane, as shown in Figure 6. It is predicted that of the formation of surfaces $NbAl_3$ (112) and Nb_7Al (110) is easier. As the impact velocity increased to 2.60 km/s, the peaks of Nb_7Al disappeared, while those of $NbAl_3$ were still retained. This suggests that the cubic crystal $(a = c)$ transitioned to a tetragonal $(a \neq c)$ structure under impact, because the shock wave was actually axial.

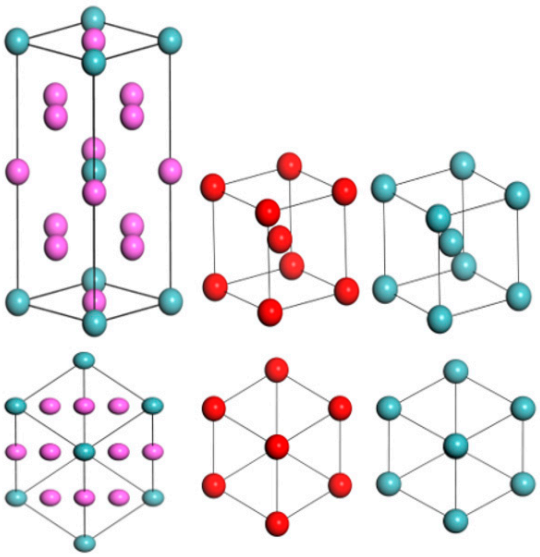


Figure 6. The atomic displacement of Nb-Al systems in plane for (**a**) $NbAl_3$ (112), (**b**) Nb_7Al (110) and (**c**) Nb (110), where the light blue is Nb, the purple is Al and the red consists of 1.725 Nb and 0.25 Al.

The crystal structures reveal that the crystal transition from cubic to tetragonal is axial under impact. When the impact pressure increased, the Nb and Al atoms moved axially, where the atoms were in plane (110) along direction [001]. The pure cubic metals transferred to Nb_7Al retained the cubic structure, and those transferred to $NbAl_3$ became tetragonal in structure. In all, those planes had strong diffraction peaks and they did not change under impact, revealing that the $NbAl_7$ and Nb_3Al alloys are easy to be synthesized from pure Nb and Al under shock waves. This is evidence to support our experiment results. Although the diffraction angles of certain crystal planes were almost equal between Al and Nb and Nb-Al alloys, the alloying process in general powder metallurgy is based on atomic diffusion, and the same is true for the shock compression of powders.

4. Conclusions

In summary, the results demonstrate that we synthesized two Nb-Al alloys via shock waves. The products after impact were measured using X-ray diffraction. In order to illustrate the micro-transition of synthesis and the characteristics of products, we used X-ray diffraction simulation to display the structural characteristics of Nb-Al systems.

These experiments and calculations provide a new synthetic pathway for Nb-Al alloys. In addition, the design of a recovery capsule was proven to be feasible.

Author Contributions: Conceptualization, C.-L.J. and Q.-J.L.; Data curation, Z.J.; Formal analysis, Z.J.; Project administration, Z.-T.L.; Software, Z.-T.L. and Q.-J.L.; Supervision, Q.-J.L.; Writing—original draft, Y.-L.T.; Writing—review & editing, C.-L.J. All authors have read and agreed to the published version of the manuscript.

Funding: This research received no external funding.

Institutional Review Board Statement: Not applicable.

Informed Consent Statement: Not applicable.

Conflicts of Interest: The authors declare no conflict of interest.

References

1. Seiler, F.; Igra, O. *Hypervelocity Launchers*; Springer International Publishing: Cham, Switzerland, 2016; pp. 3–19. [CrossRef]
2. Crozier, W.D.; Hume, W. High-Velocity, Light-Gas Gun. *J. Appl. Phys.* **1957**, *28*, 892–894. [CrossRef]
3. Dlott, D.D. New Developments in the Physical Chemistry of Shock Compression. *Annu. Rev. Phys. Chem.* **2011**, *62*, 575–597. [CrossRef] [PubMed]
4. Lexow, B.; Wickert, M.; Thoma, K.; Schäfer, F.; Poelchau, M.H.; Kenkmann, T. The extra-large light-gas gun of the Fraunhofer EMI: Applications for impact cratering research. *Meteorit. Planet. Sci.* **2013**, *48*, 3–7. [CrossRef]
5. Erskine, D.; Nellis, W.J. Shock-induced martensitic phase transformation of oriented graphite to diamond. *Nature* **1991**, *349*, 317–319. [CrossRef]
6. Sato, T.; Ishii, T.; Setaka, N. Formation of Cubic Boron Nitride from Rhombohedral Boron Nitride by Explosive Shock Compression. *J. Am. Ceram. Soc.* **1982**, *65*, c162. [CrossRef]
7. Sōma, T.; Sawaoka, A.; Saito, S. Characterization of wurtzite type boron nitride synthesized by shock compression. *Mater. Res. Bull.* **1974**, *9*, 755–762. [CrossRef]
8. Sekine, T.; He, H.; Kobayashi, T.; Zhang, M.; Xu, F. Shock-induced transformation of β-Si_3N_4 to a high-pressure cubic-spinel phase. *Appl. Phys. Lett.* **2000**, *76*, 3706–3708. [CrossRef]
9. Sekine, T.; He, H.; Kobayashi, T.; Shibata, K. Sinoite (Si2N2O) shocked at pressures of 28 to 64 GPa. *Am. Miner.* **2006**, *91*, 463–466. [CrossRef]
10. Sekine, T.; Kobayashi, T.; Li, X. Hugoniot of beta-SiAlON and high-pressure phase transitions. *J. Appl. Phys.* **2006**, *99*, 53501. [CrossRef]
11. Hanada, S. Niobium aluminides. *Curr. Opin. Solid State Mater. Sci.* **1997**, *2*, 279–283. [CrossRef]
12. Wang, N.; Du, C.; Hou, J.; Zhang, Y.; Huang, K.; Jiao, S.; Zhu, H. Direct synthesis of Nb–Al intermetallic nanoparticles by sodiothermic homogeneous reduction in molten salts. *Intermetallics* **2013**, *43*, 45–52. [CrossRef]
13. Leyarovski, E.; Leyarovska, L.; Krasnopyorov, E.; Kokot, L.; Horyń, R.; Mydlarz, T. Superconductivity and magnetic properties of Nb—Al phases: Nb2Al and NbAl3. *Eur. Phys. J. B* **1977**, *27*, 57–60. [CrossRef]
14. Papadimitriou, I.; Utton, C.; Tsakiropoulos, P. Ab initio investigation of the Nb–Al system. *Comput. Mater. Sci.* **2015**, *107*, 116–121. [CrossRef]
15. Neumeier, J.J.; Nellis, W.J.; Maple, M.B.; Torikachvili, M.S.; Yang, K.N.; Ferreira, J.M.; Summers, L.T.; Miller, J.I.; Sales, B.C. Metastable A15 phase Nb3Si synthesized by high dynamic pressure. *High Press. Res.* **1989**, *1*, 267–289. [CrossRef]
16. Yu, L.H.; Meyers, M.; Thadhani, N.N. Reaction-assisted shock consolidation of RSR Ti–Al alloys. *J. Mater. Res.* **1990**, *5*, 302–312. [CrossRef]
17. Jiao, Z.; Liu, Q.J.; Liu, F.S. Study on preparation and properties of Nb-Al superalloy under shock compression. In Proceedings of the 18th China High Pressure Science Conference, Chengdu, China, July 2016. Available online: https://cpfd.cnki.com.cn/Article/CPFDTOTAL-SCYZ201607001242.htm (accessed on 20 February 2022).
18. Jiao, Z.; Liu, Q.J.; Wang, Y.G.; Zhang, M.J.; Liu, F.S.; Chang, X.H.; Fan, D.H. Shock Compression Loading Recycling Box and Method for Preparing Material by Shock Compression, Public No. CN107008207A. Available online: https://pss-system.cnipa.gov.cn/sipopublicsearch/portal/uiIndex.shtml (accessed on 20 February 2022).
19. Hohenberg, P.; Kohn, W. Inhomogeneous Electron Gas. *Phys. Rev.* **1964**, *136*, B864–B871. [CrossRef]
20. Clark, S.J.; Segall, M.D.; Pickard, C.J.; Hasnip, P.J.; Probert, M.I.J.; Refson, K.; Payne, M.C. First Principles Methods Using CASTEP. *Z. Kristallogr. Cryst. Mater.* **2005**, *220*, 567–570. [CrossRef]
21. Jiao, Z.; Liu, Q.-J.; Liu, F.-S.; Tang, B. Structural and electronic properties of low-index surfaces of NbAl3 intermetallic with first-principles calculations. *Appl. Surf. Sci.* **2017**, *419*, 811–816. [CrossRef]
22. Lundin, C.E.; Yamamoto, A.S. Equilibrium Phase Diagram, Niobium (Columbium)-Aluminum. *Trans. Met. Soc. AIME* **1966**, *236*, 863. [CrossRef]
23. Pialoux, A.; Joyeux, M.; Cizeron, G. Étude du comportement du niobium sous vide par diffraction des rayons X à haute température. *J. Less Common Met.* **1982**, *87*, 1–19. [CrossRef]

24. Tougait, O.; Noël, H. Stoichiometry of UAl4. *Intermetallics* **2004**, *12*, 219–223. [CrossRef]
25. Suh, I.-K.; Ohta, H.; Waseda, Y. High-temperature thermal expansion of six metallic elements measured by dilatation method and X-ray diffraction. *J. Mater. Sci.* **1988**, *23*, 757–760. [CrossRef]
26. Huang, H.-J.; Jing, F.-Q.; Cai, L.-C.; Bi, Y. Grüneisen Parameter along Hugoniot and Melting Temperature of ε-Iron: A Result from Thermodynamic Calculations. *Chin. Phys. Lett.* **2005**, *22*, 836–838. [CrossRef]
27. Chau, R.; Stölken, J.; Asoka-Kumar, P.; Kumar, M.; Holmes, N.C. Shock Hugoniot of single crystal copper. *J. Appl. Phys.* **2010**, *107*, 023506. [CrossRef]
28. Jing, F.Q.; Cheng, J.X. *Principle and Technology of Dynamic High Pressure*; National Defense Industry Press: Beijing, China, 2006.